the society for solid-state and electrochemical science and technology

Journal of The Electrochemical Society

Multi-Walled Carbon Nanotubes Percolation Network Enhanced the Performance of Negative Electrode for Lead-Acid Battery

M. Saravanan, P. Sennu, M. Ganesan and S. Ambalavanan

J. Electrochem. Soc. 2013, Volume 160, Issue 1, Pages A70-A76.
doi: 10.1149/2.062301jes

Journal of The Electrochemical Society, **160** (1) A70-A76 (2013)
0013-4651/2013/160(1)/A70/7/$28.00 © The Electrochemical Society

Multi-Walled Carbon Nanotubes Percolation Network Enhanced the Performance of Negative Electrode for Lead-Acid Battery

M. Saravanan, P. Sennu, M. Ganesan, and S. Ambalavanan[z]

Electrochemical Energy System Group, CSIR-Central Electrochemical Research Institute, Karaikudi-630006, India

The discharge performance of lead-acid battery is improved by adding multi-walled carbon nanotubes (MWCNTs) as an alternate conductive additive in Negative Active Mass (NAM). We report that MWCNTs added to the negative electrode, exhibits high capacity, excellent cycling performances at 10-h rate, high rate partial state of charge (HRPSoC) cycling and various rates of discharge. It significantly reduces the irreversible lead sulfate on the NAM, increases the active material utilization and improves the electrode performance. The improvement of capacity and cyclic performance of the cell is attributed to the nanoscale dimension of the MWCNTs as additive. Subsequent characterization using high resolution transmission electron microscopy and scanning electron microscopy were carried out to understand the influence of MWCNTs on the negative electrode of lead-acid battery.
 [DOI: 10.1149/2.062301jes]

Manuscript submitted July 13, 2012; revised manuscript received October 18, 2012. Published November 7, 2012.

Development of an electrode material with high capacity and good cyclability at a high charge and discharge rate has become an important issue for present day battery technology. Most electrode materials exhibit reduced capacity and larger capacity fading at high rates. In this context, the lead–acid battery (LAB) remains an attractive choice for meeting the new requirement on account of its performance, safety, low cost, and recyclability which are the main reasons for its commercial success.[1] The lead-acid battery is ubiquitous in the global rechargeable battery market and in terms of value, its present world sales are about US$ 20 billion per annum.[2] However, the main drawback of this system is formation of irreversible lead sulphation in NAM, accompanying decrease in capacity and cycle life.[3–9]

The cycle life of the batteries is determined by the reversibility of the processes that proceed during charge/discharge. The cycle life of the battery is limited by the low charge acceptance of the negative plates. Charging of the negative plate proceeds through the following elementary processes:

Dissolution of $PbSO_4$ crystals and formation of Pb^{2+} ions on the metal surface.

$$PbSO_4 \longrightarrow Pb^{2+} + SO_4^{2-} \quad [1]$$

Diffusion of Pb^{2+} ions to the active centers where the electrochemical reaction of Pb^{2+} reduction to Pb.

$$Pb^{2+} + 2e^- \longrightarrow Pb \quad [2]$$

Electroneutralization of the SO_4^{2-} ions proceed through the diffusion and migration of H^+ ions from the bulk of the solution into the pores of the NAM.

$$SO_4^{2-} + 2H^+ \longrightarrow H_2SO_4 \quad [3]$$

If the above elementary processes are impeded, the charge process is impeded and certain quantities of $PbSO_4$ in the plates are not reduced to Pb. The accumulation of lead sulfate reduces markedly the effective surface-area and limits the performance. Moreover, the unconverted lead sulfate crystals precipitate onto the surface of the Pb phase, thus limiting the latter's contribution to the charge process and hence reducing the charge acceptance of the negative plates.[10] When the battery is not being fully charged, the lead sulfate converts from an electroactive state to the highly crystalline state. This sulfation process is irreversible and results in a loss of capacity.

To overcome this problem, predominantly in HRPSoC operations, several publications established the effect of various carbon materials addition to the negative plates of lead-acid batteries to minimize the sulphation problem.[11–16] Moreover, the function of suitable additive to the active material is to enhance the electrical conductivity and chemical stability.

The present research aims to enhance the electrochemical performance of negative plate behavior by the addition of MWCNTs. On comparing the literature, it is understood that only 40–45% of the theoretical capacity of NAM is utilized in practical LAB depending upon the type. Different methodologies have been adopted to increase the utilization efficiency of NAM.[17–22] As the active materials are converted to insulating lead sulfate on the surface, the electrode will experience an increase in resistance and volume expansion. The non-conductive layer and the poor mass transport of sulphuric acid (H_2SO_4) electrolyte to the electrode interior result in low utilization efficiency of the active material. To solve aforesaid problems, it is important to add nanostructured conducting additive in the electrode materials which will provide high surface area and good electronic conduction.

In this regard, nanostructured materials and nanotechnology offer great promise because of the unusual properties endowed by confining their dimensions and the combination of bulk and surface properties to the overall behavior.[23,24] Carbon nanotubes (CNTs) have high chemical stability, high length/diameter ratio, strong mechanical strength, high activated surface area and high conductivity which are attractive as materials for energy storage devices such as pseudo capacitors, fuel cells, and secondary batteries.[25–33] However, there are only very few reports available on the MWCNTs as an electrode and electrolyte additives in lead-acid battery.[34–36] Hojo et al. studied different weight percents of graphitized Vapor-Grown Carbon Fibers (average diameter 2–5 μm) to the positive and negative electrode and obtained better cyclic behavior in LAB.[37] Micro Bubble Technology, Inc. (MBTI) based in South Korea, developed CNT battery technology.[38]

MWCNTs enhance the electrochemical properties of the NAM by first acting as a conductive support ideal for electron transportation and secondly stabilize the electrode structure with a good electric contact between the spongy lead/lead sulfate particles during the charge–discharge process. The nanostructured conducting additives increases the electric conductivity of active mass with sufficient percolation network to achieve appropriate conductive paths. We found that the electrochemical performance of lead-acid battery using MWCNTs as conductive additive were obviously higher than those using conventional carbon black (CB) as conducting additive in the same amount.

This article aims to provide a useful survey of recent progress on characterizations of MWCNTs as an additive of negative electrode materials for lead-acid batteries.

Experimental

MWCNTs with 40–50 nm of diameter and 5–15 μm of length purity: >99%, purchased from SRL chemical Ltd, were used as conductive additive for NAM for this experiment. In order to completely get rid of transition metal impurities, CNTs were further purified – first in concentrated HNO_3 (70%) under ultrasonication for 2 h and then in 2 M HNO_3 for 2 h, followed by DI water wash. Metallic impurities are removed from MWCNT as per standard procedure.[39] The presence

[z]E-mail: vananambu456@yahoo.co.in

of impurities in MWCNTs may affect the LAB system significantly by accelerating gas evolution.

Electrode preparation and characterization.— The positive electrode was conventional lead dioxide electrode. The dimensions of the positive and negative plates made from Pb-Ca alloy were of 45 mm × 50 mm × 2.0 mm and 45 mm × 50 mm × 1.2 mm respectively. Dry mixing of the MWCNTs (0.25 wt%) with leady oxide before negative paste preparation resulted in a significant improvement in electrochemical performance of the lead-acid cell. The acid treated MWCNTs was divided into three equal parts and dry mixed with leady oxide one by one with a time duration of 5 min each to make sure that the MWCNTs dispersion is uniform in the entire leady oxide. After addition of H_2SO_4 to the leady oxide - MWCNTs mixture, the formed paste is stirred continuously for several minutes, which generates friction among the particles of the viscous paste mass.[40] Due to this friction the MWCNTs may dispersed uniformly in the lead paste.

The CB added negative electrode was prepared as per standard protocol. Two set of test cells (2 V/2Ah) were assembled with MWCNTs and CB each added separately in NAM. The plates were cured and formed as per conventional technologies. The test cells were assembled with 1 negative and 2 positive plates per cell, with PVC separator. The cells were filled with 40 mL of 1.25 sp.gr sulphuric acid (H_2SO_4). The performance of the cells was limited by the negative plate.

A series of experiments were carried out to investigate the capability of MWCNTs in enhancing the conductivity and performance of the negative electrode. The same was compared with CB (0.25 wt%) added NAM. One set of CB and MWCNTs added cells were subjected to 10 h rate cycling and also discharged to various current densities at room temperature. The 10 h rate discharge measurements were performed up to a discharge depth of 100%. An overcharge of 110% of the previous discharge capacity was set as the boundary condition for the recharge. In addition, one more set of cell performance was evaluated under simulated HRPSoC a condition, using a simplified profile imitating micro-hybrid driving mode.[40–42] In this study, the HRPSoC cycling was done by discharging the respective cells at C_1 rate to 50% of the C_1 capacity. This is followed by respective 1 minute charge and 1 minute discharge steps at the $2C_1$ rate with interval of 10s rest. This was repeated until the cell reached a lower discharge voltage of 1.83 V or when the upper voltage limit of 2.83 V. The above-described cycling steps comprise of one cycle-set of the test. After this cycle set, the cell was fully re-charged (to 100% SoC) and their C_{20} capacity was measured followed by second cycle-set.

The charge–discharge tests were carried out using Bitrode life cycle tester. The morphology and microstructure of the NAM were characterized by scanning electron microscopy (SEM, Hitachi model S-3000H) high resolution transmission electron microscopy (HRTEM, JEOL JEM-2100) and X-ray diffraction (XRD, X'pert PRO PAN) analysis. The pristine and HNO_3 treated MWCNTs were characterized by Raman spectroscopy (Renishaw RM1000-Invia) with a laser excitation energy of 638 nm. The electronic conductivity of NAM pellet was measured by four-probe method at room temperature. The electrochemical impedance spectroscopy (IM6) was performed in the frequency range of 10 mHz–100 kHz at an AC voltage of 5 mV.

Results and Discussion

Raman spectra.— Fig. 1a and 1b shows the obtained Raman spectrum for pristine and acid treated MWCNTs. Three characteristic peaks of MWCNTs are observed namely D band at 1332 cm^{-1}, G-band at 1579 cm^{-1} and G'- band at 2664 cm^{-1} as shown in Fig. 1a and 1b. After HNO_3 treatment (Fig. 1b), these characteristic peaks are still present, proving that the acid treatment does not damage the structure of MWCNTs. The ratio of I_D/I_G is increased for functionalized MWCNTs as compared to pristine MWCNTs. It means that the HNO_3 treatment of MWCNTs breaks some bonds and inserts functional groups that can be considered as defects on the structure. The graphitized carbon contains sp^2 hybrid bonding, which is positively correlated with the electronic conductivity of carbon and the disordered carbon mainly corresponds to sp^3 hybrid bonding.

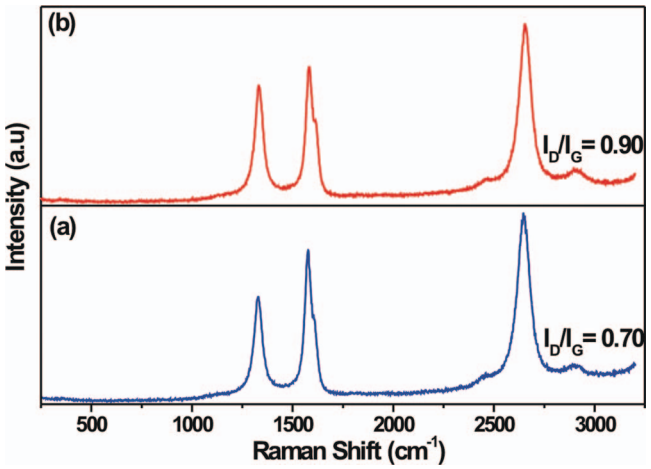

Figure 1. Raman spectrum for (a) pristine and (b) acid treated MWCNTs.

Cycle-life studies on lead-acid cells (10-h rate).— The Fig. 2a shows that an increase in capacity was observed with MWCNTs as conductive additive as compared to the CB added cell. This due to higher electronic conductivity of MWCNTs (1.67×10^3 Sm^{-1}) as compared with CB (5.26×10^2 Sm^{-1})[43] and the one dimensional structure of MWCNTs favor electrons delivery through the negative plate. Moreover, the MWCNTs added cell exhibits excellent cyclability with no noticeable fade compared to the CB added cell as seen in Fig. 2a. In the case of the MWCNTs added cell, the capacity increases gradually during the initial several cycles, then stabilizes at about 2.25 Ah, and shows a good retention of capacity on cycling. Therefore, the discharge performance of LAB improves subsequently by using MWCNTs as conductive additive. This indicates that the utilization of the active materials may also contribute to the capacity rise in the electrodes. But in the case of CB added cell there is no initial capacity rise as noticed in the MWCNTs added cell and the first discharge capacity of CB added cell is 2.25 Ah. Moreover, the decrease in capacity is significantly very rapid for CB added cell compared to MWCNTs added cell. By contrast, capacity fade takes place after 80 cycles for the electrode without MWCNTs. Furthermore, the cell showed a rapid capacity fade and delivered 1.25 Ah at 180^{th} cycle. It is explicit that this material demonstrated relatively poor capacity retention. It is easily understood that formation of irreversible lead sulfate is one of the main reasons for capacity decay of negative electrode. Though MWCNTs added cell did not show any prominent capacity fade, the slight decrease can be observed as the cycles progress.

The discharge performance curves under different discharging current densities for the cells were also shown in Fig. 2b. Under all discharge current densities, the discharge capacity of MWCNTs added cell was much higher than those of CB added cell. The voltage plateau of cells with MWCNTs as conductive additive was also higher than the one using CB as conductive additive at high discharge rate. This most beneficial effect due to MWCNTs can change the specific surface of NAM and facilitate the high current density. It is well known that the specific surface of NAM is determined not only by the specific surface of lead but also by the specific surface of the additive.[14]

The discharge profiles of the 5th, 70th and 110th cycles for the CB and MWCNTs added cells cycled at 10-h rate were shown in Fig. 2c and 2d. From the curves, we can see that the MWCNTs added electrodes show the best discharging performance with the highest discharge capacity. There was no decline in the capacity in MWCNTs added cells during cycling. On the other hand, CB added cells shows a decreasing capacity with increasing cycle numbers as clearly revealed in Fig. 2c. During charge, the major part of the lead sulfate crystal was converted to spongy lead in the case of MWCNTs added

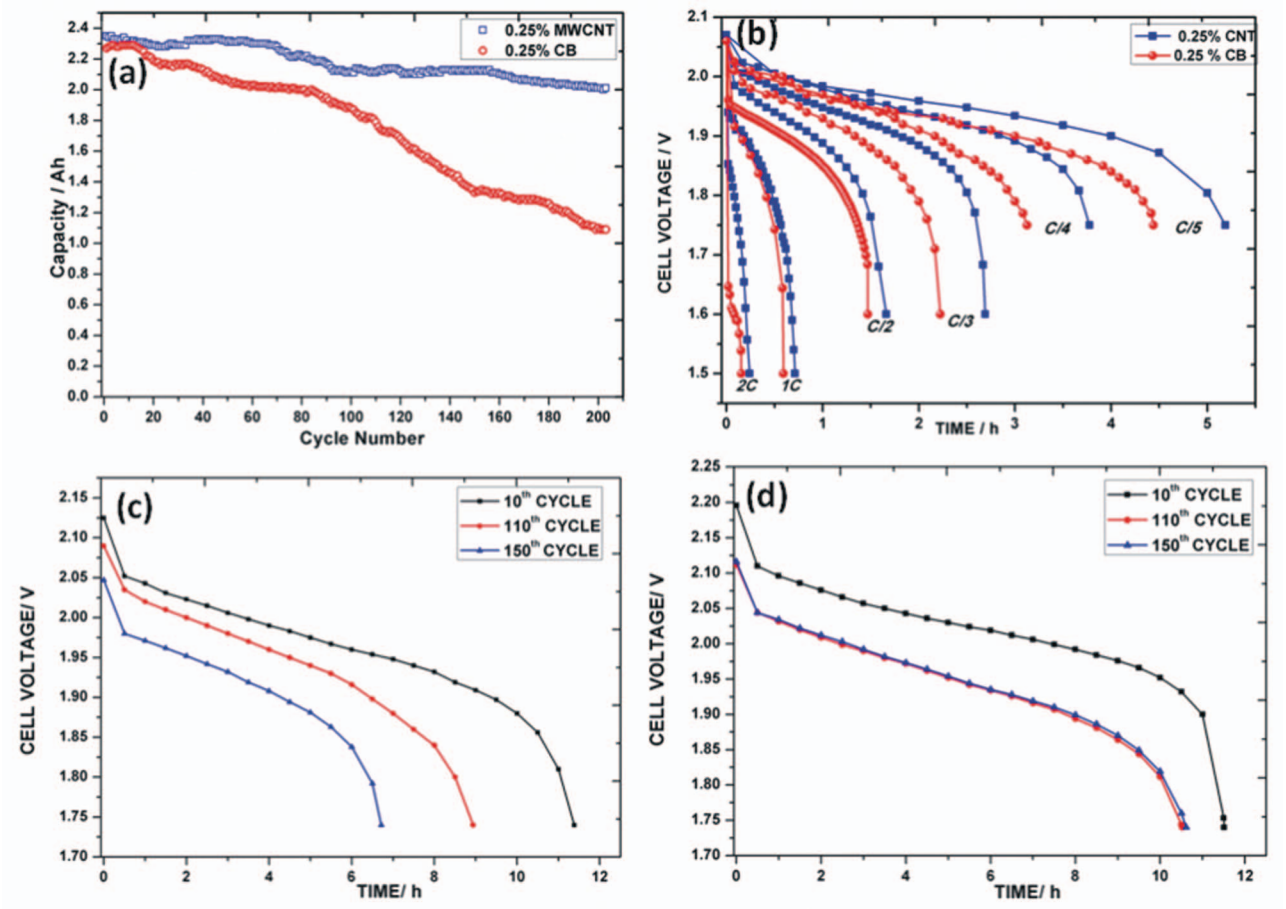

Figure 2. (a) Comparative cycling (10-h rate) performance of CB and MWCNTs added cell. (b) The rate capability of CB and MWCNT added cell at different current densities. (c-d) The comparison of the discharge curves of cells with CB and MWCNTs added cells at 10-h rate.

cell. The MWCNTs network contributes to the transfer of electrons to Pb^{2+} ions that lead to the formation of Pb much effectively as compared to CB added NAM. High resistance to oxidation of MWCNTs may also contribute the improved utilization of the NAM and stable capacity retention of the cell. Numerous author report that CNTs are more resistant to electrochemical oxidation than CB in H_2SO_4.[44–46] Interestingly, in our experiment, CNTs were added in the negative electrode and its oxidation is negligible in the potential window studied. In addition, MWCNTs may tune the electrochemical activity of the electrode although the detailed mechanism involved is not yet fully understood.

Based on the data in Fig. 2a-2d, we assume that in the MWCNTs added NAM that contribute to building the operating NAM structure proceed with a high degree of reversibility. On charge, the operating structure of NAM is recovered completely thus ensuring longer cycle life. On the other hand, the conductive MWCNTs network also plays a positive role to improve the electrochemical performance of negative electrode by endowing an unexpected electronic path for fast and stable charge transfer and lowering the internal resistance of the cell. The results indicate that introducing MWCNTs into NAM is an effective way to improve both the cycling performance and rate performance of the cell. The superior rate performance of the cell with MWCNTs is due to the electronically conductive matrix provided by the MWCNTs as shown in Fig. 3.

The charge profiles for the CB and MWCNTs added cells cycled at 10-h rate were shown in Fig. 4. Addition of MWCNTs to the negative paste lowers the charge voltage. This charging curve indicates that the randomly distributed MWCNTs are absorbed on the lead surface and facilitate the electron transfer at lower potential. Furthermore, in the CB added cell there is a strong polarization at the start of recharge. The voltage increases with progression of charge. This is because, the internal resistance of the cell becomes large. Dissolution of lead sulfate at the negative electrode is unable to provide sufficient soluble lead ions during charge. As a result, the resistance of the cell may increases and the charge voltage reaches higher compared with MWCNT added cell.

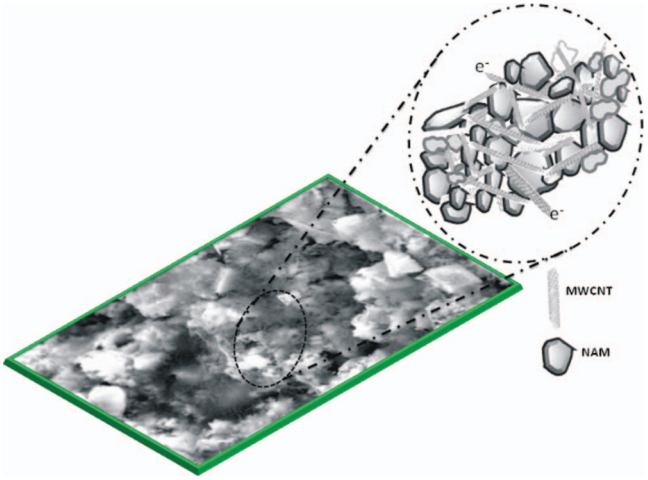

Figure 3. Schematic of a tentative mechanism for the formation of conducting network with MWCNTs added NAM.

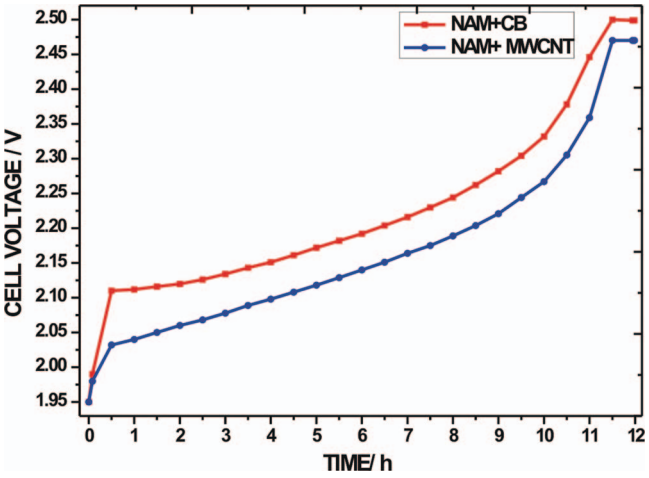

Figure 4. Charge profiles for the CB and MWCNTs added cells at 10-h rate.

Cycle life of cells in HRPSoC condition.— Although most electronics require only moderately high charge/discharge rates, newer applications, such as regenerative braking in hybrid electric vehicles, (i.e., the ability to charge and discharge very fast) has been difficult to accomplish with LAB. To overcome this problem Pavlov et al. developed various additive added negative plate for HRPSoC application.[14,15,40,47] Inadequate electronic conductivity could still become an impediment to achieve HRPSoC performance. During the 1 min charge and 1 min discharge pulses at a current rate of $2C_1$ employed during the HRPSoC test, the charge and discharge reactions occurring mainly on the surface layers of the NAM. Moreover, high resistance to oxidation of MWNCTs slightly tune the Pb to $PbSO_4$ formation. This indicates that surface of the NAM partially have some amounts of electrochemically active Pb at the end of HRPSoC discharge. The remaining non-oxidized part of Pb conducts the electric current from the grid to throughout the NAM if the electrode is being discharged,[15] so that the reduction process takes place much efficiently. The high aspect ratio of nanotubes allows for more effective conducting paths within the NAM. Furthermore it can build a strong adhesion with Pb particles and lowers the ohmic resistance. Submillimeter long MWCNTs can minimize the number of junctions in the electrode network and electrode resistance hence attain efficient charge process. MWCNTs are adsorbed on the lead surface and it may create a new electrochemically active interface that enhances the electrochemical process. This interface easily allows the electron transfer.[14] It is clear that, nanostructured additive offer improved energy storage capacity and charge/discharge kinetics, as well as better cyclic stabilities due to their high surface area for faradaic reaction and short distance for mass and charge diffusion. Furthermore, randomly distributed MWCNTs contributed in maintaining the electronic conduction around the NAM that favors the reduction process.

Fig. 5a shows the experimental data for the end-of-charge/discharge cell voltages during the HRPSoC test for cells with CB and MWCNTs added NAM. The CB added cell was highly polarized during charge in the second cycle-set. These results indicate that the negative plates are heavily sulphated during cycling. Moreover, this cell delivered 4400 micro-cycles in the first cycle-test and reduced to 1550 micro-cycles before reaching the lower voltage limit of 1.83 V. Interestingly, cells with MWCNTs in NAM have the best cycle life performance, between 13688 to 7000 micro-cycles resulting in enhancement of HRPSoC performance compared to the CB added electrode as shown in Fig. 5a. The small particle size can aid to realize a better electrochemical utilization of the materials. Nanostructured materials are found to demonstrate unique properties in terms of electrode conductivity and particle to particle contact due to their nanometer sizes where electron tunneling is quicker than micron-sized particles. Therefore, employing nanosized particles as electrode for

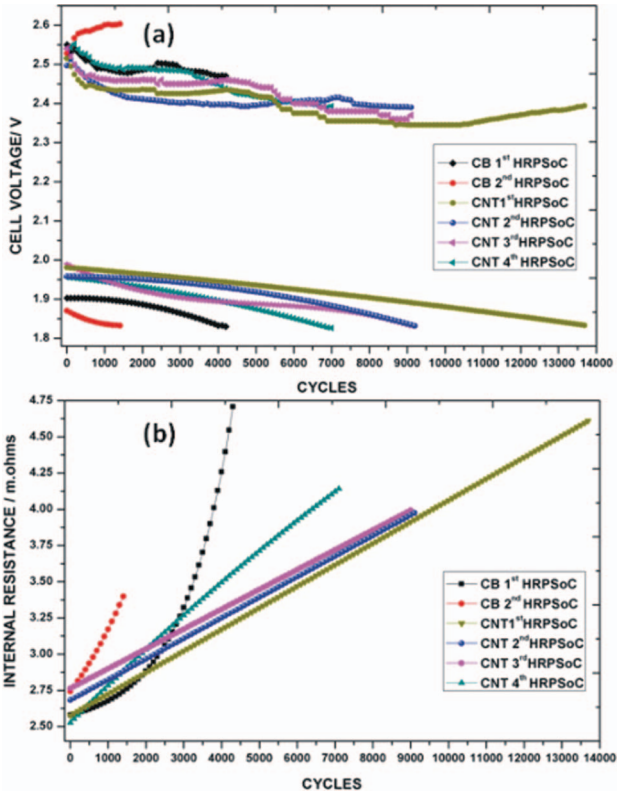

Figure 5. (a) End of Charge and discharge profile for CB and MWCNTs added cells on HRPSoC cycling, (b) Internal resistance in CB and MWCNTs added cells in respective HRPSoC cycle.

such application would certainly help to achieve such high rate capability within the cell. Adding nanosized conductive materials into the electrode material can improve the electronic conductivity and morphological stability in high rate discharge. Moreover, internal resistance of CB added cell indicate that there is a steep raise as revealed in Fig. 5b.

The behavior of the cell capacity after each HRPSoC cycle set is shown in Fig. 6 After the each HRPSoC cycle test, the capacity (C_{20}) of CB added cell has dramatically decreased. Interestingly, MWCNTs added cell after subsequent HRPSoC cycle sets shows a relatively

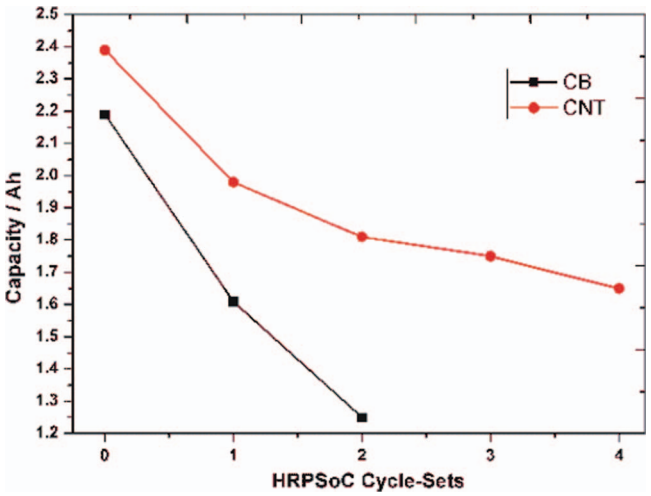

Figure 6. Cell capacity after each HRPSoC cycle set.

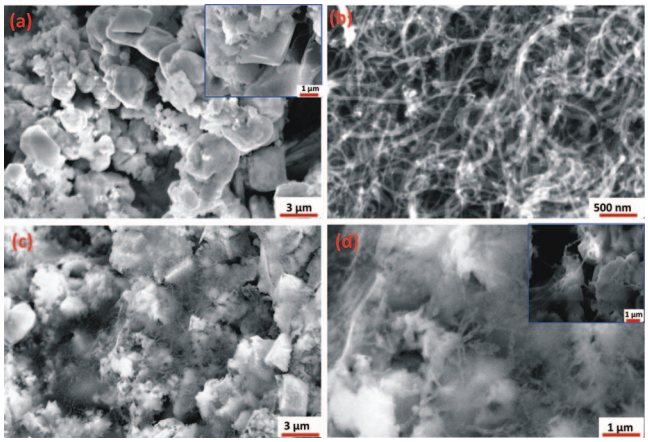

Figure 7. SEM images of (a) CB added NAM, (b) Pristine MWCNTs and (c) & (d) nanoscale networked NAM with MWCNTs, illustrating the strong interaction between the NAM and MWCNTs. The inset in (a&d) is an enlarged SEM images. (After 70 charge/discharge cycles).

small decrease in discharge capacity as compared to the initial capacity values.

Scanning electron microscopy of NAM with CB and MWCNTs.— The SEM images of CB and MWCNTs added NAM are shown in Fig. 7, and it is observed that MWCNTs are connected with active mass particles in series and it is interlaced all particles together to form a network wiring in the NAM. Thus an effective network percolation is formed (Fig. 7c-7d). The formation of NAM/ MWCNTs hierarchical structure is further confirmed in the micrograph presented as inset (Fig. 7d). These structures demonstrate superior energy storage performance and good structural stability after cycling. It must be noted here that the presence of MWCNTs helps to maintain a porous lead structure with a high surface area and electronic conductivities of the intra- and inter-Pb particles during cycling.

SEM observation shows a general view of MWCNTs added NAM as compared with CB added NAM. Fig. 7c-7d shows randomly aligned MWCNTs with an outer diameter of approximately 40–50 nm and a length of 10–15 µm at different magnification levels. The morphology of the CB added NAM was also observed in order to confirm the morphological changes after the cycling process as shown in Fig. 7a which clearly reveals the distribution of unconverted lead sulfate crystals. We can also observe that MWCNTs added NAM shows needle-like structures that are not present in the CB added NAM.(Fig. 7a and 7c) This suggests that many of the individual MWCNTs on each active material are highly accessible for electrochemical cycling processes, which significantly increases the available electroactive surface area and increase the electrochemical performance. The high aspect ratio of nanotubes allows for more effective conducting paths to the current collector[48,49] and exhibits good structural stability during the charge-discharge process.

A material to be considered as a conductive additive, it must provide a conduction path from the current collector to the active material through the thickness of the electrode material. CB particles are nearly spherical and have an average diameter of ~40 nm. Considering this particle size many hundreds of CB particles would be required to create a conductive path that will spread on the whole electrode thickness. The principal resistance in such a system is likely to be the many particle-to-particle contacts. In contrast, the MWCNTs used in the present study had an average length of 10 µm. The number of nanotubes required to spread the electrode would be one to two orders of magnitude fewer than CB particles, with correspondingly fewer particle-to-particle contacts.[50,51] This suggests that the electronic resistance of electrodes containing MWCNTs is expected to be much lower. Moreover, the porous structure of MWCNTs permits electrolyte access throughout the NAM.

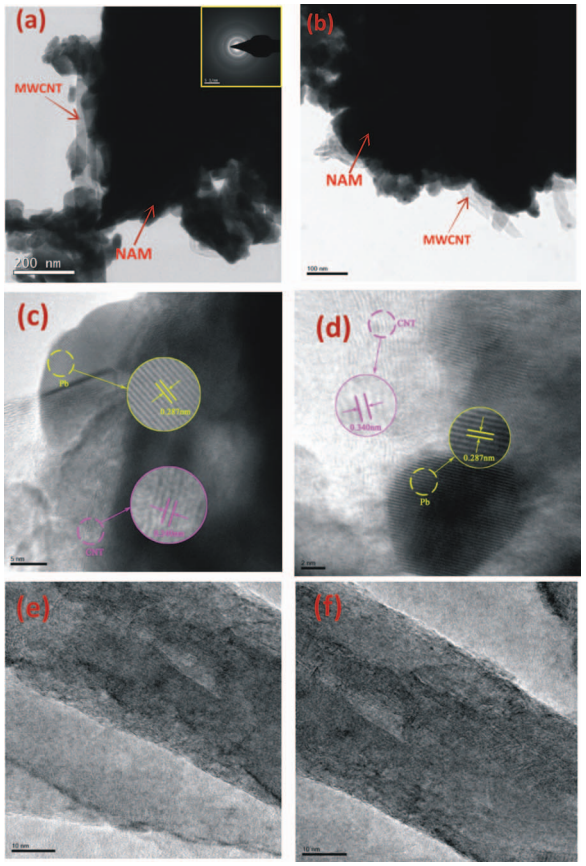

Figure 8. TEM (a&b) and HRTEM (c&d) images of MWCNTs with NAM (e-f) HRTEM images of MWCNTs (After 70 charge/discharge cycles).

Transmission electron microscopy of NAM with MWCNTs.— TEM analysis was carried out to determine the microstructure of the MWCNTs added NAM. To the best of our knowledge TEM images of NAM with MWCNTs are reported for the first time. It is well known that the electrochemical performance is not only highly dependent on the intrinsic crystalline texture and surface properties, but also greatly related to the morphology and assembled structure of active materials with conductive additives. In the case of MWCNTs as alternate to traditional carbon materials as conductive additive, it has been found that the formed resilient conductive networks of NAM with MWCNTs (Fig. 8a-8b) are expected to contribute to the establishment of electrical contact throughout the electrode. It is well known that the MWCNTs with high graphitic degree are favorable for a good electrical conductivity.

Fig. 8a-8d shows a uniform dispersion of MWCNTs into the NAM which is crucial to achieve higher performance. Thus it is suggested that the nanotubes not only decorate the surface, but also incorporate and intrude into the pores and bulk of the NAM particles, thus forming a hierarchical architecture. The corresponding SAED pattern presented as inset (Fig. 8a) This structure yields promising electrode performance, as this mesopores can serve as facilitator for fast electron transfer within the active material. Furthermore, such images indicate good adhesion between the NAM and the MWCNTs, which is important for good performance of the electrode. In addition, the active sites at the edge significantly contribute to the superior electrochemical behavior as shown in Fig. 8a and 8b. This structure allows the penetration by the electrolyte and consequently facilitating faradaic reactions.

High-resolution transmission electron microscopy (HRTEM) constitutes a very powerful tool for detecting nanometer-scale changes in structure and morphology. The HRTEM images were analyzed to obtain interplanar (*d*) spacings, revealed by lattice fringes, using

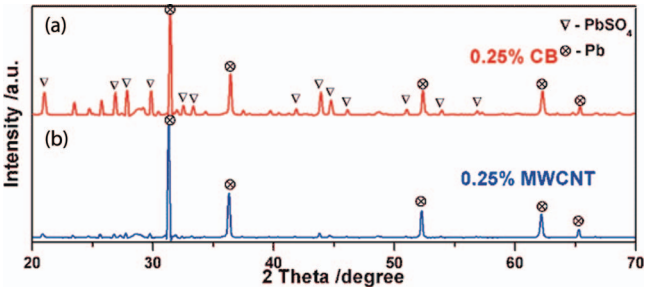

Figure 9. Typical XRD patterns of the samples: (a) CB, (b) MWCNTs added NAM (After 70 charge/discharge cycles).

Digital MicroAnalysis software.[52] The bright contrast in the image corresponds to the presence of heavy elements (Pb). As shown in Fig. 8c and 8d. lattice fringes can be observed from the HRTEM, indicating crystallization of the Pb and MWCNTs. The measured interplanar spacing of 0.287 nm correspond to the (111) planes of Pb with different growth directions[53] in the middle layer and 0.340 nm of MWCNTs in the outer layer, respectively. Fig. 8e and 8f shows the HRTEM images of the MWCNTs.

Conductivity of NAM.— The electronic conductivity of negative active mass has not been clearly elucidated yet. In this study conductivity was measured for the prepared battery negative electrode after the formation process. A small pellet was removed from negative electrode and subjected to four probe measurement. As expected, the electronic conductivities of the MWCNTs added NAM (4420 $S.cm^{-1}$) are much higher than that of CB added NAM (3140 $S.cm^{-1}$). The obtained value is relatively low compared with the literature value.[54–57] Since the pellet was not compressed at high pressure, the small voids might have created inside the pellet and the NAM gets easily oxidized in the atmosphere covered with a thin oxide layer which may be the reason for low conductivity. Moreover, the formed material from pasted plates is a complex mixture containing very small amount of basic lead sulfates, lead oxide, barium sulfate, lignosulfonate, etc in which some additives may be responsible for reduced conductivity.

Crystal structure of NAM.— X-ray diffraction was performed to determine the phase of the charged state of NAM after 70 cycles. The result relies on the formation of irreversible lead sulfate which is very low in the presence of MWCNTs as a conductive additive in NAM (Fig. 9). The presence of irreversible lead sulfate on the surface of the CB added NAM implies that certain amount of lead sulfate has not been converted back to spongy lead during charge. This suggests that incomplete reduction of $PbSO_4$ to Pb was confirmed with CB added NAM. A significant amount of $PbSO_4$ was observed during cycling in the CB added cell. The origin of which could be associated with conductivity problems that make difficult for the proton and electron transfer between particles. In the XRD pattern we have not observed any CB and MWCNTs phase due to the low amount of addition.

Impedance measurement.— Electrochemical impedance spectroscopy tests were performed for both CB and MWCNTs added cells (10 and 110 cycles) to understand the behavior and resistance associated with the electrodes. MWCNTs added electrode material exhibits much lower resistance than the CB added electrode, as shown in Fig. 10. As a result CB added cell displays the expected behavior, in that, after 110 charge/discharge cycles, the cell impedance increased. This may be due to the accumulation of a poorly conductive irreversible lead sulfate formed on the electrode surface. This observation demonstrates that electronic conduction plays a critical role in controlling the electrochemical properties of lead acid batteries. The MWCNTs suppresses the resistive growth arising from a reaction of the negative electrode surface with the electrolyte. Thus MWCNTs added electrode provides a high surface and large contact area between NAM and grid; therefore, the total resistance of MWCNTs added cell is smaller than that of CB added cell.

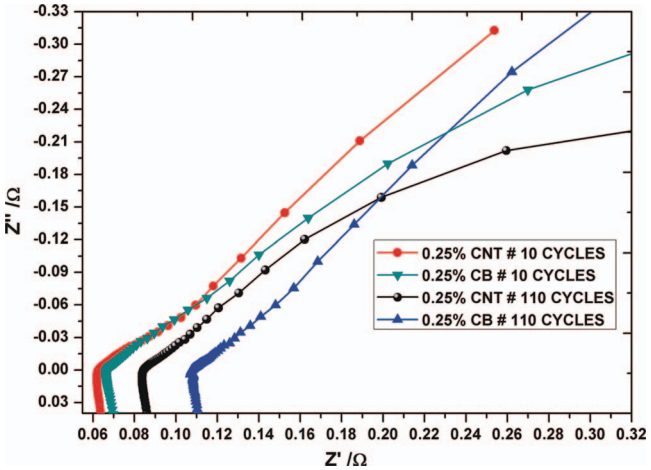

Figure 10. Electrochemical impedance spectra for CB and MWCNTs added cells in respective 10-h rate cycle.

Conclusions

MWCNTs have been employed as the conductive additive in the negative plate of rechargeable lead-acid batteries showing improvement in the capacity of the electrodes as compared to CB added electrode. The enhanced performance is due to the significant specific electroactive area formed by MWCNTs network within the active material. This performance enhancement effect is attributed to the improved electrochemical accessibility and decrease in inert irreversible lead sulfate zones provided by the interpenetrating conductive MWCNTs networks present in the NAM. Furthermore, the structure of MWCNTs is more adaptable to the homogeneous dispersion with NAM than other carbon materials, adding an optimum amount of MWCNTs into the NAM can achieve a higher cycle life. There is evidence to believe that MWCNTs more effectively prevent the irreversible lead sulfate particles and hence therefore retain the enhanced electrical properties. On the basis of this result and discussion, it could be concluded that the capacity fade was effectively reduced in the lead acid cell. MWCNTs play a critical role in controlling the particle composition, size, morphology, and the overall electrochemical properties and performances of LAB. It could be clearly seen that MWCNTs were suitable additive for NAM as it enhances the efficient contact between active material and form a percolating conducting network. Nanomaterial additives also offer great potential to develop next generation lead-acid negative plate with high energy densities. The results here give clear evidence of MWCNTs networks in improving the electrochemical performance of negative electrode for lead-acid batteries.

Acknowledgments

The authors are thankful to the Council of Scientific and Industrial Research (CSIR), India for the support to carry out this work.

References

1. J. Garche, *Phys. Chem. Chem. Phys.*, **3**, 356 (2001).
2. R. M. Dell and D. A. J. Rand, *Understanding Batteries*, Cambridge, UK: Royal Society of Chemistry, (2002).
3. Y. Guo, S. Tang, G. Meng, and S. Yang, *J. Power Sources*, **191**, 127 (2009).
4. A. Cooper and P. T Moseley, *J. Power Sources*, **113**, 200 (2003).
5. L. T. Lam, N. P. Haigh, C. G. Phyland, and A. J. Urban, *J. Power Sources*, **133**, 126 (2004).
6. A. Cooper, L. T. Lam, P. T. Moseley, and D. A. J. Rand, in: D. A. J. Rand, et al., (Eds.), *Valve-Regulated Lead-Acid Batteries*, Elsevier BV, (2004).

7. P. Ruetschi, *J. Power Sources*, **127**, 33 (2004).
8. D. Boden, J. Arias, and F. A. Fleming, *J. Power Sources*, **95**, 277 (2001).
9. H. Dietz, H. Niepraschk, K. Wiesener, J. Garche, and J. Bauer, *J. Power Sources*, **46**, 191 (1993).
10. D. Pavlov and P. Nikolov, *J. Electrochem. Soc.*, **159**, A1215 (2012).
11. K. Nakamura, M. Shiomi, K. Takahashi, and M. Tsubota, *J. Power Sources*, **59**, 153 (1996).
12. M. Shiomi, T. Funato, K. Nakamura, K. Takahashi, and M. Tsubota, *J. Power Sources*, **64**, 147 (1997).
13. P. T. Moseley, R. F. Nelson, and A. F. Hollenkamp, *J. Power Sources*, **157**, 3 (2006).
14. D. Pavlov, T. Rogachev, P. Nikolov, and G. Petkova, *J. Power Sources*, **191**, 58 (2009).
15. D. Pavlov, P. Nikolov, and T. Rogachev, *J. Power Sources*, **196**, 5155 (2010).
16. P. T. Moseley, *J. Power Sources*, **191**, 134 (2009).
17. N. E. Bagshaw, *J. Power Sources*, **67**, 105 (1997).
18. R. David Prengaman, *J. Power Sources*, **144**, 426 (2005).
19. D. Pavlov, G. Petkova, and T. Rogachev, *J. Power Sources*, **175**, 586 (2008).
20. C. V. D'Alkaine, A. Carubelli, and M. C. Lopes, *J. Appl Electrochemistry*, **30**, 585 (2000).
21. C. S. Dai, B. Zhang, D. L. Wang, T. F. Yi, and X. G. Hu, *Mater. Chem. and Phys.*, **99**, 431 (2006).
22. M. A. Karimi, H. Karami, and M. Mahdipour, *J. Power Sources*, **160**, 1414 (2006).
23. A. Manthiram, V. A. Murugan, A. Sarkar, and T. Muraliganth, *Energy & Environ Sci*, **1**, 621 (2008).
24. D. Tasis, N. Tagmatarchis, A. Bianco, and M. Prato, *Chem. Rev*, **106**, 1105 (2006).
25. R. A. H. Niessen, J. de Jonge, and P. H. L. Notten, *J. Electrochem. Soc.*, **153**, A1484 (2006).
26. Il-Hwan Kim, Jae-Hong Kim, Young-Ho Lee, and Kwang-Bum Kim, *J. Electrochem. Soc.*, **152**, A2170 (2005).
27. Il-Hwan Kim, Jae-Hong Kim, Byung-Won Cho, and Kwang-Bum Kim, *J. Electrochem. Soc.*, **153**, A1451 (2006).
28. Chia Ying Lee, Huei Mei Tsai, Huey Jan Chuang, Seu Yi Li, Pang Lin, and Tseung Yuen Tseng, *J. Electrochem. Soc.*, **152**, A716 (2005).
29. M. Gnanavel, Manu U. M. Patel, A. K. Sood, and Aninda J. Bhattacharyya, *J. Electrochem. Soc.*, **159**, A336 (2012).
30. S. R. Sivakkumar and Dong-Won Kim, *J. Electrochem. Soc.*, **154**, A134 (2007).
31. Haiyan Zhang, Yiming Chen, Yuting Chen, Shuangping Yi, Zhifeng Zeng, Haiyan Chen, and Xiaojuan Fu, *J. Electrochem. Soc.*, **157**, A1164 (2010).
32. Sakae Takenaka, Hiroshi Matsumori, Hideki Matsune, Eishi Tanabe, and Masahiro Kishida, *J. Electrochem. Soc.*, **155**, B929 (2008).
33. Zhe Tang, How Y. Ng, Jianyi Lin, Andrew T. S. Wee, and Daniel H. C. Chua, *J. Electrochem. Soc.*, **157**, B245 (2010).
34. W. Xing-hua, Z. Xiao-bing, Y. Wei-liang, T. Jun-jun, G. Yun-fang, and T. Xin-yong, *J. Material Science & Engineering*, **25**, 932 (2007), http://d.wanfangdata.com.cn/Periodical_clkxygc200706031.aspx.
35. K. Mickaa, M. Calabek, P. Baca, P. Krivak, R. Labus, and R. Bilko, *J. Power Sources*, **191**, 154 (2009).
36. R. Zhao, G. Shi, H. Chen, A. Ren, X. Fang, S. Liu, and J. Hu, in *proc. of "13th Asian Battery conference"* Venetian Macao Resort Hotel 1-4 September 2009, Machu, China.
37. E. Hojo, J. Yamashita, K. Kishimoto, H. Nakashima, and Y. Kasai, *YUASA-JIHO. Tech Rev.*, **72**, 8 (1992), http://www.gs-yuasa.com/us/technic/backnumber.html.
38. http://www.ecolocap.com/newsEvents.php?news = 25.
39. P.-X. Hou, C. Liu, and H-M. Cheng, *Carbon*, **46**, 2003 (2008).
40. D. Pavlov, P. Nikolov, and T. Rogachev, *J. Power Sources*, **195**, 4444 (2010).
41. M. Saravanan, M. Ganesan, and S. Ambalavanan, *J. Electrochem Soc.*, **159**, A452 (2012).
42. D. P. Boden, D. V. Loosemore, M. A. Spence, and T. D. Wojcinski, *J. Power Sources*, **195**, 4470 (2010).
43. H. Dai, *Surf. Sci.*, **500**, 218 (2002).
44. L. Li and Y. Xing, *J. Power Sources*, **178**, 75 (2008).
45. Y. Shao, G. Yin, J. Zhang, and Y. Gao, *Electrochim. Acta*, **51**, 5853 (2006).
46. X. Wang, W. Li, Z. Chen, M. Waje, and Y. Yan, *J. Power Sources*, **158**, 154 (2006).
47. D. Pavlov, P. Nikolov, and T. Rogachev, *J. Power Sources*, **195**, 4435 (2010).
48. L. Hu, D. S. Hecht, and G. Gruner, *Nano. Lett.*, **4**, 2513 (2004).
49. Y. X. Zhou, L. B. Hu, and G. Gruner, *Appl. Phys. Lett.*, **88**, 123109 (2006).
50. Q. Lin and J. N. Harb, *J. Electrochem. Soc.*, **151**, A1115 (2004).
51. U. D. Weglikowska, J. Yoshida, N. Sato, and S. J. Roth, *J. Electrochem. Soc.*, **158**, 174 (2011).
52. R. J. Martin-Palma, L. Pascual, P. Herrero, and J. M. Martines-Duart, *Appl. Phys. Lett.*, **81**, 25 (2002).
53. Z. Chen, Y. Cao, J. Qian, X. Ai, and H. Yang, *J. Solid State Electrochem*, **16**, 291 (2012).
54. H. Metzendorf, *Materials Chemistry*, **4**, 601 (1979).
55. W. Mindt, *J. Electrochem. Soc.*, **116**, 1076 (1969).
56. E. C. Dimpault-Darcy, T. V. Nguyen, and R. E. White, *J. Electrochem. Soc.*, **135**, 278 (1988).
57. D. M. Bernardi and M. K. Carpenter, *J. Electrochem. Soc.*, **142**, 2631 (1995).